

An avoided Lifshitz-type semimetal-semiconductor transition?: Infrared conductivity of elemental bismuth under pressure

N. P. Armitage,^{1,2} Riccardo Tediosi,² F. Lévy,² E. Giannini,² L. Forro,³ and D. van der Marel²

¹*Department of Physics and Astronomy, The Johns Hopkins University, Baltimore, MD 21218, USA.*

²*Département de Physique de la Matière Condensée, Université de Genève,*

quai Ernest-Ansermet 24, CH1211 Genève 4, Switzerland.

³*Ecole Polytechnique Fédérale de Lausanne, Switzerland.*

(Dated: June 16, 2022)

The application of pressure to elemental bismuth reduces its conduction-valence band overlap, and results in a semimetal-semiconductor (SMSC) transition around 25 kbar. This transition is nominally of the topological ‘Lifshitz’ Fermi surface variety, but there are open questions about the role of interactions at low charge densities. Using a novel pressure cell with optical access, we have performed an extensive study of bismuth’s infrared conductivity under pressure. In contrast to the expected pure band behavior we find signatures of enhanced interaction effects, including strongly coupled charge-plasmon (plasmaron) features and a plasma frequency that remains finite up to the transition. These effects are inconsistent with a pure ‘Lifshitz’ band-like transition. We postulate that interactions play a central role in driving the SMSC transition.

PACS numbers: 71.45.-d, 78.40.Kc, 78.20.-e, 78.30.-j

Since the seminal work of Wigner in 1930’s, it has been believed that the large relative electron interactions in low density charge systems manifest themselves in a variety of novel phases like electronic crystals, correlated heavy electron fluids, and inhomogeneous states¹⁻³. In principle elemental bismuth is a model system to investigate such physics. It is a semimetal with small valence and conduction band overlap, three small electron Fermi pockets (at the L points), and a hole Fermi pocket (at the T point), which gives an equal (small) number of both charge species at E_F . A material of much long term interest with many interesting properties⁴, bismuth has recently been found to host a variety of exotic electronic phenomena, including phase transitions at high field to a ‘valley-ferromagnetic’ state⁵, signatures of charge fractionalization in the ultra-quantum high field limit⁶, and strongly coupled electron-plasmon ‘plasmaron’ features in the optical spectra⁷. Recently, it also has been claimed that $\text{Bi}_{1-x}\text{Sb}_x$ alloys are ‘topological insulators’, with robust topologically protected surface states⁸.

Among its remarkable phenomena, bismuth undergoes an interesting semimetal-semiconductor (SMSC) transition with the application of modest pressures (≈ 25 kbar)⁹. This transition is relatively under investigated⁹⁻¹¹, but unlike more conventionally discussed Mott- or Anderson-style metal-insulator transitions driven by local interactions or disorder respectively, it is believed to be driven by a reduction of the semimetal conduction and valence band overlap Δ (See Fig. 1). As the overlap decreases, Fermi surfaces shrink and eventually vanish. Within a non-interacting purely band point of view this is an electronic topological transition of the ‘Lifshitz’ variety¹². It is unclear however what role is played by electronic correlations on the approach to the transition when charge densities are low. Do interactions dominate resulting in a strongly correlated liquid state? Perhaps the continuous topological ‘Lifshitz’

band transition is superseded by a 1st-order discontinuous transition¹³ or a phase like an electronic crystal^{1,2}, excitonic insulator¹⁴, or inhomogeneous state³.

Bismuth has an $A7$ rhombohedral lattice. Its exceptional electronic properties originate in the small deviation of this structure from higher symmetry simple cubic. It can be formed from the successive distortions of two interpenetrating fcc sublattices; first a small relative displacement along the body diagonal, and then a small rhombohedral shear along the same direction. The body-diagonal displacement doubles the real space lattice constant and gaps states at the chemical potential and reduces electronic energy in the usual fashion. In a hypothetical structure with only the Peierls-like body diagonal displacement, the gapping would be complete and the material a semiconductor with zero near- E_F density of states¹⁵. The additional symmetry lowering from finite rhombohedral shear allows valence and conduction band overlap¹⁵. Such considerations allow us to understand the effect of pressure. Bismuth has a strongly anisotropic compressibility, with the c -axis 3 times more elastic than the perpendicular direction¹⁶. Since the angle associated with the rhombohedral shear determines the unit cell volume, it couples strongly to pressure. Increased pressure drives the angle back towards the more symmetric cubic value (60°) and decreases the band overlap, driving the material through a SMSC transition.

In this Letter, we present the results of an infrared conductivity study of bismuth up to its pressure tuned SMSC transition. We observe colossal changes in bismuth’s optical conductivity as the material approaches the SMSC transition. Near the critical pressure we find evidence for correlation effects and a plasma frequency that stays finite through the transition showing that this transition is likely not of a pure Lifshitz variety. Our work also represents an important proof of principle for the technique in which we have demonstrated the abil-

ity to perform reliable far-infrared conductivity measurements under pressure and at low temperatures without the use of a synchrotron.

The single-crystal bismuth sample used in this work was grown by a modified Bridgman-Stockbarger technique⁷. We confirmed with X-ray diffraction that the mirror-like cleavage surfaces were [110] planes perpendicular to the trigonal axis. Measurements were performed with a standard Bruker 66 IR spectrometer. Ambient pressure spectra were measured in our usual optical cryostat⁷. Using a novel kerosene filled piston-cylinder cell¹⁷ equipped with a large 2 mm diamond window we performed infrared optical reflection experiments on a sample mounted in contact with the window. A 2° angular miscut of the diamond allowed us to separate the contribution coming from the front and back interfaces. The unusually large optical access and a special kinematic mounting for the cell allowed us to measure down into far-infrared. The pressure dependent resistance of an InSb chip was used to determine the pressure at temperatures down to 10 K.

The determination of the complex conductivity $\sigma(\omega)$ or dielectric function $\varepsilon(\omega)$ consists of three main steps¹⁸. First, using a rigorous calibration procedure, the signal was corrected for the stray light reflected at the diamond/vacuum interface. Next, the data are combined with the reflectivity measured outside the pressure cell to provide the absolute reflectance of the diamond/sample interface at room temperature and for each pressure. Finally, the relative change of the intensity as a function of temperature gives the reflectivity $R(\omega, T)$. The complex optical constants are generated via a Kramers-Kronig consistent fitting procedure of $R(\omega)$ constrained by ambient pressure ellipsometry between 0.7 and 4.5 eV¹⁹.

In Fig. 1 we show the effective reflectivity of the bismuth-air interface at a number of different pressures and temperatures. As discussed previously⁷, the reflectivity of bismuth exhibits a sharp plasma edge whose frequency decreases rapidly with temperature. In the optical response of simple metals, the plasma edge is exhibited when $\varepsilon_1(\omega) = 0$, which is satisfied self-consistently at the screened plasma frequency $\tilde{\omega}_p = \omega_p / \sqrt{\varepsilon_\infty(\tilde{\omega}_p)}$. Here ε_∞ is the contribution to dielectric constant from everything except the Drude term and ω_p^2 is the Drude spectral weight $4\pi ne^2/m_b$ (n is the charge density and m_b is the band mass.). $\tilde{\omega}_p$ occurs at anomalously small values in bismuth, due to both its low charge density and exceptionally large $\varepsilon_\infty \approx 85 - 95$. The rapidly decreasing plasma frequency as a function of temperature reflects the freezing out of charges at low temperature (Fig. 2(a)).

Superficially the effect of pressure looks similar to the effect of temperature. However in this case the plasma edge decreases due to a smaller band overlap. The behavior is summarized in Fig. 2(b), where we plot as a function of pressure at different temperatures the plasma frequency ω_p of the Drude component from a Drude-Lorentz fit to the reflectivity data. At low pressure the

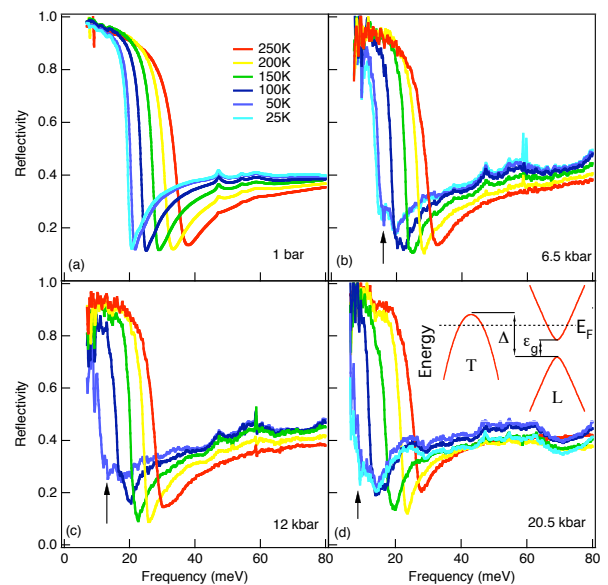


FIG. 1: (Color) Reflectivity of an effective bismuth-air interface at a number of different pressures. The small 47 meV feature is an artifact of the IR beam splitter. Small black arrows denote the ‘plasmaron’ feature.

data looks to be roughly consistent with a vanishing free charge density extrapolating to zero near the known critical pressure. However at higher pressures, the experimental data extrapolate to a finite value at the transition point. We will return to this point (and the overlaid theoretical curves) below.

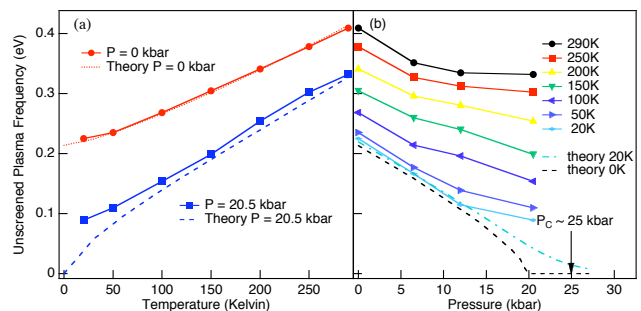


FIG. 2: (Color) (a) Temperature dependence of the plasma frequency at ambient pressure and at 20.5 kbar. (b) Plasma frequency as a function of pressure at various temperatures. Theoretical curves match the experimental ones exceedingly well except in the regime of the critical pressure at low temperature. Note that the Drude-Lorentz fits are very over constrained and there is less than 5% uncertainty in these numbers.

In Figs. 3(a) and (b) we plot the real parts of the low temperature (20 K) optical conductivity and dielectric function at different pressures. Although the gross

aspects of the spectra are as expected for a metallic system with a small number of free charges, a more detailed analysis shows a number of interesting fine features. At 6.5 kbar we observe a plateau in the conductivity and an inflection point in the dielectric function around 18 meV. These features systematically move to lower energies as the pressures increases (see arrows). The inflection point in the real part of the dielectric function also becomes progressively more pronounced as the pressure increases. This behavior may anticipate a second zero-crossing of ϵ_1 which could occur in proximity to the SMSC transition.

These features, which are found in the vicinity of the screened plasmon frequency, are evidence for the coupled electron-plasmon “*plasmaron*” feature that we have previously observed in the ambient pressure spectra⁷. This is an electron-boson interaction similar in character to electron-phonon or electron-magnon interactions, except here the collective mode is purely electronic. As noted by Lundqvist^{20,21} the plasmon pole contribution to the quasi-particle self-energy has a similar form to that of the polaron problem. Indeed the term *plasmaron* follows from this analogy. Note that such effects should only be visible in the conductivity in a system which breaks Galilean invariance, which here is afforded by the simultaneous presence of electrons and holes. Such coupling effects are particularly significant in bismuth due to its anomalously low plasmon frequency. They become even more pronounced as the charge density vanishes close to the SMSC, showing the increased role of interactions at low charge densities. Note that these plasmaron features are visible in the raw reflectivity curves themselves; a structure additional to the usual plasma minimum develops near the plasma edge at high pressures and low temperature as denoted by the arrows in Fig. 1.

As may be expected, the plasmaron features show up dramatically in the loss function $\text{Im} \frac{-1}{\epsilon(\omega)}$ itself, as an additional peak or shoulder near the usual plasmon peak as shown in Fig. 3(c). With increasing pressure, spectral weight shifts from the main plasmon peak to the “*plasmaron*” derived peak. Such shifts of spectral weight from primary to satellite peaks are consistent with increasing interactions exhibiting themselves in an enhancement of the optical mass as one approaches the SMSC transition.

This plasmaron coupling also manifests itself directly in the low energy physics. In Fig. 3(d) we plot the Drude scattering rate determined from the Drude-Lorentz fits, which at finite pressure has a distinct non-monotonic form. It is interesting to note that it has the same qualitative dependence as the DC resistivity itself⁹. From the DC data alone, it is not clear if a non-monotonic resistivity could be caused by the competing effects of a decreasing scattering rate and decreasing carrier density. Here we show that there are unusual non-monotonic dependencies in the scattering rate itself. This shows that electron-electron interactions in the form of plasmon coupling plays an increasingly important role as one approaches the nominal Lifshitz transition. Also note that the high temperature scattering rate actually *decreases*

at high pressures.

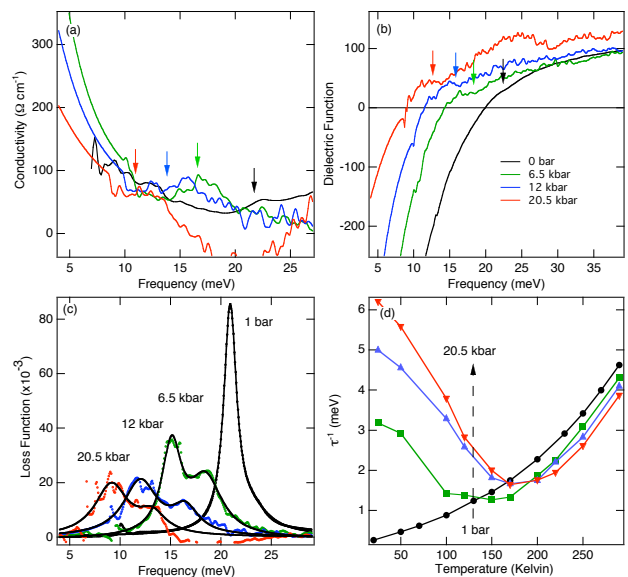


FIG. 3: (Color) (a) Real optical conductivity for 6.5, 12, and 20.5 kbar at 20K. Arrows denote position of ‘*plasmaron*’ absorption. The small negative shift in the 20.5 kbar spectra is an artifact of the calibration procedure. (b) Real part of the dielectric function. (c) Low temperature (20K) loss function. (d) Temperature dependence of the scattering rate as a function of temperature at different pressures. Data below 7 meV is an extension of the fit in the generalized Kramers-Kronig analysis.

As noted above and shown in Fig. 2, although the low temperature plasmon frequency is significantly suppressed as one approaches the nominal critical pressure, a reasonable extrapolation of the data does not appear to go to zero at p_c as would be expected if the free carrier density vanishes *à la* Lifshitz. In Fig. 2, overtop the experimental data we plot a band calculation of the pressure and temperature dependent plasma frequency from the Drude spectral weight. The calculation was performed taking into account the three relevant charge species: (1) heavy holes (*hh*) at the T point with a standard massive dispersion ($\epsilon_k^{hh} = \hbar^2 k^2 / m_k^{hh}$), (2) light electrons (*le*) and (3) their light hole (*lh*) counterparts at the three-fold degenerate L point, for which the energy dispersion is: $\epsilon_k = \Delta - \epsilon_g/2 \pm \sqrt{\epsilon_g^2/4 + \hbar^2 |\vec{k} \cdot \vec{v}_F|^2}$ where ϵ_g is the direct gap between the two bands. The effective mass-tensor of the light carriers near the gap is defined by $\vec{m} = \epsilon_g / (2\vec{v}_F^2)$. Band parameters are given in Table I. The SMSC transition is governed by the band overlap ($-\Delta$) of the heavy hole and light electron bands. By adjusting the chemical potential the calculation fulfills charge neutrality: $n_{hh} + n_{lh} = n_{le}$. The plasma frequency ω_p follows from the general relation: $\omega_p^2 = 4\pi e^2 \sum_j \left[\sum_k n_k^j / m_k^j \right]$ where the j is a band index

and $\hbar^2/m_k = -\partial^2\epsilon_k/\partial k^2$.

Heavy hole masses	$m_a = 0.064, m_b = 0.064, m_c = 0.69$
Light particle velocities	$v_F^1 = 1080, v_F^2 = 71.1, v_F^3 = 669$
Band overlap Δ	$\Delta = \Delta^0 \times (1 - 0.07T/\Delta^0 - p/p_c)$ $\Delta^0 = -40$ meV, $p_c = 20$ kbar
Direct gap ϵ_g	$\epsilon_g = \epsilon_g^0 \times (1 + 2.5e^{-4T^2/\epsilon_g^0})$ $\epsilon_g^0 = 15$ meV

TABLE I: Parameters used for the plasma frequency calculation. The ‘0’ index stands for zero temperature and pressure; masses are given in units of the free electron mass; a,b,c are respectively the binary, bisectrix and trigonal axis; the (2,3) plane is tilted 6.23° relatively to (b,c); velocities are in km/s . The band parameters were adopted from fits of the Hall coefficient, magneto-optics, cyclotron resonance and Shubnikov-de-Haas oscillations²²⁻²⁴.

At zero pressure, the calculation fits the plasma frequency exceedingly well over the entire temperature range while at 20.5 kbar there is a substantial disagreement at low temperature (Fig. 2(a)). From Fig. 2(b) the discrepancy is enhanced as the SMSC transition is approached. The calculation predicts the SMSC transition to occur at 20 kbar, which is completely missed by the experimental data. Note that there is a reasonable amount of uncertainty in the pressure dependence of the band parameters²²⁻²⁴ and so the calculation should not be taken too literally, but in any case the experimental ω_p does not appear to extrapolate to zero at the known p_c near 25 kbar.

The appearance of strong correlation features in the spectra and the finite value of ω_p on the approach to the SMSC transition at 25 kbar shows that pure Lifshitz-like behavior is superseded by some other - presumably interaction driven - effects. A naive estimate of the effective dimensionless interaction parameter r_s at ambient pressure is quite small if one considers the large lattice ϵ_∞ found at the screened plasma frequency and a small effective mass (for the holes $r_s = \frac{me^2}{n^{1/3}\hbar^2 4\pi\epsilon_\infty\epsilon_0} \approx 0.2$). However, the appropriate ϵ_∞ for the bare interaction strength is not the $q = 0$ one relevant at the plasma edge, but instead one relevant at short distances that is

likely much smaller. This is reasonable when one considers that the typically cited large ϵ_∞ derives from low energy, but highly dispersive interband transitions at the L point²⁵ and moreover, that the dominant interaction in these systems has a short-range excitonic character. A larger r_s means that at lower densities near the transition, interactions could become quite significant.

A number of possibilities exist for the physics that supersedes the Lifshitz transition. The system’s charge density may not go to zero continuously¹³, but instead may undergo a first-order interaction driven instability in which it collapses discontinuously to zero at p_c ^{14,26}. Alternatively, the finite value of ω_p near p_c could come from the system breaking up into charge rich and charge poor regions (but still locally neutral so that $n = p$) in a manner similar to electron-hole droplets in semiconductors²⁷ or so-called ‘microemulsions’³. In this scenario, the transition at p_c would essentially be one of percolative character. Another possibility is that the charge density remains finite because the transition at p_c is actually Wigner crystallization. It has been shown that there is a strong tendency for charge crystallization in two component plasmas at densities where r_s is even of order unity²⁸. This is far below that necessary in one component systems. Such tendencies are reinforced in systems with a large mass asymmetry such as bismuth. Although throughout our experimental range the system clearly remains metallic, plasmon features could be the manifestation of enhanced ‘Wigner liquid’ correlations on the approach to such a transition²⁹. Finally, excitonic scattering³⁰ or correlations¹⁴ near the SMSC transition could play a role as they are believed to dominate at similar densities in $TmSe_{0.45}Te_{0.55}$ ³¹. Despite the clear signatures of interaction effects we have found there is clearly more work to be done on this interesting system and we hope that our work is stimulating in that regard.

We would like to thank K. Behnia, A. MacDonald, O. Vafek, and Z. Wang for helpful discussions and R. Gaal for technical support. This work is supported by the SNSF through Grant No. 200020-125248 and the National Center of Competence in Research (NCCR) ‘Materials with Novel Electronic Properties-MaNEP.’ NPA was supported by NSF DMR-0847652 and the NSF International Research Fellows Program.

¹ E. Wigner, Phys. Rev. **46**, 1002 (1934).

² D. M. Ceperley and B. J. Alder, Phys. Rev. Lett. **45**, 566 (1980).

³ B. Spivak et al., arXiv:0905.0414v1 (2009).

⁴ V. S. Édel’man, Adv. in Phys. **25**, 555 (1976).

⁵ L. Li et al., Science **321**, 547 (2008).

⁶ K. Behnia, L. Balicas, and Y. Kopelevich, Science **317**, 1729 (2007).

⁷ R. Tediosi, N. P. Armitage, E. Giannini, and D. van der Marel, Phys. Rev. Lett. **99**, 016406 (2007).

⁸ D. Hsieh et al., Nature **452**, 970 (2008).

⁹ D. Balla and N. B. Brandt, Soviet Physics JETP **20**, 1111 (1965).

¹⁰ E. Itskevich and L. Fisher, Soviet Physics JETP **25**, 66 (1968).

¹¹ W. Kraak, R. Herrmann, and H. Haupt, physica status solidi (b) **109**, 785 (1982).

¹² I. M. Lifshitz, JETP **11**, 1130 (1960).

¹³ M. Kaganov and A. Moebius, ZHURNAL EKSPERIMENTALNOI I TEORETICHESKOI FIZIKI **86**, 691 (1984).

¹⁴ B. I. Halperin and T. M. Rice, Rev. Mod. Phys. **40**, 755 (1968).

- ¹⁵ A. B. Shick et al., Phys. Rev. B **60**, 15484 (1999).
- ¹⁶ G. K. White, J. Phys. C: Solid State Phys **5**, 2731 (1972).
- ¹⁷ I. Kézsmárki et al., Phys. Rev. B **71**, 193103 (2005).
- ¹⁸ R. Tediosi, Phd. Thesis, *University of Geneva* (2008).
- ¹⁹ A. B. Kuzmenko, Rev. Sci. Instrum. **76**, 083108 (2005).
- ²⁰ B. Lundqvist, Phys. Kondens. Materie **6**, 193 (1967).
- ²¹ B. Lundqvist, Phys. Stat. Sol. **32**, 273 (1969).
- ²² B. Norin, Physica Scripta **15**, 341 (1977).
- ²³ E. E. Mendez, A. Misu, and M. S. Dresselhaus, Phys. Rev. B **24**, 639 (1981).
- ²⁴ G. E. Smith, G. A. Baraff, and J. M. Rowell, Phys. Rev. **135**, A1118 (1964).
- ²⁵ P. Alstrom and H. Nielsen, Journal of Physics C: Solid State Physics **14**, 1153 (1981).
- ²⁶ Y. Yamaji, T. Misawa, and M. Imada, Journal of the Physical Society of Japan **75**, 094719 (2006).
- ²⁷ C. Jeffries and L. Keldysh, eds., Electron-hole droplets in semiconductors (Nauka, Moscow, 1998).
- ²⁸ M. Bonitz et al., Phys. Rev. Lett. **95**, 235006 (2005).
- ²⁹ V. Sa-yakanit, M. Nithisoontorn, and W. Sritrakool, Physica Scripta **32**, 334 (1985), URL <http://stacks.iop.org/1402-4896/32/334>.
- ³⁰ F. X. Bronold, H. Fehske, and G. Röpke, J. Phys. Soc. Jpn **76**, 27 (2007).
- ³¹ P. Wachter, B. Bucher, and J. Malar, Phys. Rev. B **69**, 094502 (2004).